



1

2

3

4 **Arctic sea ice-free season projected to extend into fall**

5

6

7

8 Marion Lebrun¹, Martin Vancoppenolle¹, Gurvan Madec¹, François Massonnet^{2,3}

9 ¹ Sorbonne Université (UPMC Paris 6), LOCEAN-IPSL, CNRS/ IRD/MNHN, Paris, France

10 ² Earth and Life Institute, Université catholique de Louvain, Louvain-la-Neuve, Belgium

11 ³ Earth Sciences Department, Barcelona Supercomputing Center, Barcelona, Spain

12

13

14

15

16

17

18

19

20

21 Marion Lebrun, Laboratoire d'Océanographie et du Climat, IPSL Boite 100, 4 Place Jussieu, 75252

22 Paris CEDEX 05, France.



23 **Abstract**

24

25 The recent Arctic sea-ice reduction is associated with an increase in the ice-free season duration,
26 with comparable contributions of earlier retreat and later freeze-up. Here we show that within the
27 next decades, the trends towards later freeze-up should progressively exceed and ultimately double
28 the trend towards an earlier ice retreat date. This feature is robustly found in a hierarchy of climate
29 models and is consistent with a simple mechanism: solar energy is absorbed more efficiently than it
30 can be released in non-solar form until freeze-up. Based on climate change simulations, we envision
31 an increase and a shift of the ice-free season towards fall, which will affect Arctic ecosystems and
32 navigation.



33 **1. Introduction**

34 Arctic sea ice has strikingly declined in coverage (Cavalieri and Parkinson, 2012), thickness
35 (Kwok and Rothrock, 2009; Renner et al., 2014; Lindsay and Schweiger, 2015) and age (Maslanik et
36 al., 2011) over the last four decades. CMIP5 global climate and Earth System Models simulate and
37 project this decline to continue over the 21st century (Massonnet et al., 2012; Stroeve et al., 2012) due
38 to anthropogenic CO₂ emissions (Notz and Stroeve, 2016), with a loss of multi-year ice estimated for
39 2040-2060 (Massonnet et al., 2012), in the case of a business-as-usual emission scenario.

40 Less Arctic sea ice also implies changes in ice seasonality. Over the satellite period (1979-
41 2013), the Arctic open water season duration has increased by >5 days per decade (Parkinson, 2014),
42 generally due to earlier ice retreat and less so due to later-freeze-up (Stammerjohn et al., 2012). There
43 are regional deviations in the contributions to a longer open water season duration, most remarkably
44 in the Chukchi and Beaufort Seas where later freeze-up takes over (Johnson and Eicken, 2016;
45 Serreze et al., 2016), which has been attributed to increased oceanic heat advection from Bering Strait
46 (Serreze et al., 2016). Such changes in the seasonality of Arctic ice-covered waters reflect the
47 response of the ocean surface energy budget to warming. Indeed, warming and ice thinning imply
48 earlier surface melt onset and ice retreat (Markus et al., 2009; Stammerjohn et al., 2012; Blanchard-
49 Wrigglesworth et al., 2010). Besides, a shift towards later freeze-up, tightly co-located with earlier
50 retreat is observed, especially where negative sea-ice trends are large (Stammerjohn et al., 2012;
51 Stroeve et al., 2016). This has been attributed to the ice-albedo feedback, namely to the combined
52 action of (i) earlier ice retreat, implying lower surface albedo and (ii) higher annual solar radiation
53 uptake by the ocean. Such mechanism (Stammerjohn et al., 2012) explains the ongoing delay in
54 freeze-up date of a few days per decade from the estimated increase in solar absorption (Perovich et
55 al., 2007), in accord the observed in situ increase in the annual SST maximum (Steele et al., 2008;
56 Steele and Dickinson, 2016).



57 The observed increase in the ice-free season duration should continue over the next century, as
58 projected by the CESM-Large Ensemble (Barnhart et al., 2016), but important inter-annual variability
59 will likely be superimposed on this signal. Other CMIP5 ESMs likely project a longer ice season as
60 well, for sure in the Alaskan Arctic where they have been analysed (Wang and Overland, 2015). In
61 both these studies, the simulated future increases in the ice-free season duration seem dominated by
62 the later freeze-up rather than by earlier retreat as in contemporary observations. Such behaviour
63 remains unexplained and could be a peculiarity of the CESM-Large Ensemble simulations and of the
64 Alaskan Arctic. In all cases, it is important to investigate how plausible a future shift into fall of the
65 Arctic open water season would be, because of direct ecosystem (e.g., Laidre et al., 2015) and socio-
66 economic implications (e.g., on shipping, Smith and Stephenson, 2013).

67 In this study, we aim at better quantifying the potential changes in Arctic sea ice seasonality
68 and understanding the associated mechanisms. We first revisit the ongoing changes in Arctic sea ice
69 retreat and freeze-up dates using satellite passive microwave records, both at inter-annual and multi-
70 decadal time scales. We also analyse, for the first time over the entire Arctic, all CMIP5 historical
71 and RCP8.5 simulations covering 1900-2300 and study mechanisms at play using a one-dimensional
72 ice-ocean model.



73 **2. Methods**

74 We analyse the recent past and future of sea ice seasonality by computing a series of
75 diagnostics based on satellite observations, Earth System Models and a simple ice-ocean model.

76

77 **2.1 Data sources**

78 Passive microwave sea ice concentration (SIC) retrievals, namely the GSFC Bootstrap
79 SMMR-SSM/I quasi-daily time series product, over 1980-2015 (Comiso, 2000, updated 2015), are
80 used as an observational basis. We also use CMIP5 Earth System Model reconstructions and future
81 projections of SIC. Because of high inter-annual variability in freeze-up and retreat dates and because
82 some models lose multi-year ice only late into the 21st century, we retain the 9 ESMS simulations that
83 pursue RCP8.5 until 2300 (first ensemble member, Table 1). Analysis focuses on 1900-2200,
84 combining historical (1900-2005) and RCP8.5 (2005-2200) simulations. 2200 corresponds to the
85 typical date of year-round Arctic sea ice disappearance (Hezel et al., 2014). We also extracted the
86 daily SST output from IPSL-CM5A-LR. All model outputs were interpolated on a 1° geographic grid.

87 Finally, to investigate how mean state biases may affect ESM simulations, we also included
88 in our analysis a 1958-2015 ice-ocean simulation performed with the NEMO-LIM 3.6 model (Rousset
89 et al., 2015), driven by the DFS5 atmospheric forcing (Dussin et al., 2015). NEMO-LIM 3.6 is very
90 similar to the ice-ocean component of IPSL-CM5A-LR, except that (i) horizontal resolution is twice
91 as high (1° with refinement near the poles and the equator) and (ii) a weak sea surface salinity
92 restoring is applied. Such a simulation, not only performs generally better than a free-atmosphere
93 ESM run in terms of seasonal ice extent (Uotila et al., 2017), but also has year-to-year variations in
94 close alignment with observations, a feature that is intrinsically beyond the capabilities of a free-
95 atmosphere ESM.

96

97



98 2.2 Ice seasonality diagnostics

99 We use slightly updated computation methods for ice retreat (d_r) and freeze-up (d_f) dates, as
100 compared with previous contributions (Parkinson, 1994; Stammerjohn et al., 2012; and Stroeve et al.,
101 2016). Ice retreat date (d_r) is defined as the first day of the year where SIC drops below 15%, whereas
102 freeze-up date (d_f) is the first day of the year where SIC exceeds this threshold (Stroeve et al., 2016).
103 Trends in d_r and d_f and cross-correlations have low sensitivity to the value of the SIC threshold. All
104 previous studies recognise that a typical 5-day temporal filtering on the input ice concentration is
105 required to get rid of short-term dynamical events (Stammerjohn et al., 2012; Stroeve et al., 2016).
106 By contrast, we use 15 days, in order to reduce noise due to short-term ice events, which barely affects
107 trends in d_r and d_f (see Table S1). Another important issue is the reference time axis, which varies
108 among authors. To circumvent the effect of the d_f discontinuity between Dec 31 and Jan 1, we define
109 the origin of time on Jan 1, and count d_f negatively if it falls between Jul 1 and Dec 31. Jul 1 is a safe
110 limit, because there is no instance of freeze-up date between early June and late July in the satellite
111 record or in CMIP5 simulations. The length of the ice-free season is defined as the period during
112 which SIC is lower than 15%.

113 The same seasonality diagnostics are computed from model outputs. Yet, since the long-term
114 ESM simulations used here only have monthly SIC outputs, we compute the ice seasonality
115 diagnostics based on monthly SIC fields linearly interpolated daily. Such operation drastically
116 reduces error dispersion, but introduces a small systematic bias on d_r (early bias) and d_f (late bias),
117 on the order of 5 ± 6 days, which was determined from daily interpolation of monthly averaged
118 satellite data, see Table S2. This small systematic bias in model ice retreat and freeze-up dates likely
119 contributes to the mean model bias compared to satellite data (Table 1, Fig. 1), but remains small
120 compared to the long-term signals analysed throughout this paper.

121 The ice seasonality diagnostics over the recent past and their spatial distribution are reasonably
122 well captured by the mean of selected CMIP5 models (Fig. 2). Larger errors in the individual models



123 (Fig. S1) are associated with an inaccurate position of the ice edge. Overall, ESMs tend to have a
124 shorter open water season than observed, which is tangible in the North Atlantic and North Pacific
125 regions and can be related to the tendency of our model subset to overestimate sea ice. Such an
126 interpretation is supported by the good consistency between the simulated ice seasonality diagnostics
127 with observations in the NEMO-LIM 3.6 run, as compared with IPSL-CM5A-LR (Fig. S1).

128

129 **2.3. Trends in freeze-up and retreat dates, and freeze-up vs. retreat amplification coefficients**

130 Trends in ice retreat and freeze-up dates were calculated for each satellite or model pixel, from
131 the slope of a least-square fit over a given period, using years where both d_r and d_f are defined. If the
132 number of years used for calculation of the trend is less than 1/3 of the considered period, a missing
133 value is assigned. 1/3 compromises between spatial and temporal coverage of the considered time-
134 series (see Tab. S1).

135 To describe the relative contribution of freeze-up and retreat dates to changes in open water
136 season duration, we introduce a first diagnostic, termed the *long-term freeze-up vs. retreat*
137 *amplification coefficient* ($R_{f/r}^{long}$). $R_{f/r}^{long}$ is defined as minus the ratio of trends in ice freeze-up to trends
138 in ice retreat dates. The sign choice for $R_{f/r}^{long}$ is such that positive values arise for concomitant long-
139 term trends toward later freeze-up and earlier retreat. By definition, $R_{f/r}^{long} > 1$ if the long-term trend in
140 freeze-up date exceeds the long-term trend in retreat date in a particular pixel, otherwise $R_{f/r}^{long} < 1$.
141 Note that for $R_{f/r}^{long}$ to be meaningful, we restrict computations to pixels where trends in both d_r and
142 d_f are significant at a specified confidence level. $p=0.05$, i.e. a 95% confidence interval gives the most
143 robust value but heavily restricts the spatial coverage, especially for CMIP5 outputs. By contrast,
144 $p=0.25$, i.e. a 75% confidence interval slightly expands coverage, but loses some robustness. In order
145 to study the shorter term association between retreat and freeze-up, we introduce a second diagnostic,
146 termed the *short-term freeze-up vs retreat amplification coefficient* ($R_{f/r}^{short}$). $R_{f/r}^{short}$ is defined by



147 applying the same reasoning to inter-annual time scales, as minus the linear regression coefficient
148 between de-trended freeze-up and ice retreat dates. Such definition warrants comparable
149 interpretation for $R_{f/r}^{short}$ and $R_{f/r}^{long}$.

150 All trends and freeze-up vs. retreat amplification coefficients given in the rest of the text are
151 median (\pm inter-quartile range), taken over the seasonal ice zone. We use non-parametric statistics
152 because the distributions are not Gaussian.

153

154 **2.4 1D model**

155 We use the Semtner (1976) zero-layer approach for ice growth and melt above an upper
156 oceanic layer taking up heat, whereas snow is neglected. The model simplifies reality by assuming
157 constant mixed-layer depth, no horizontal advection in ice and ocean, and no heat exchange with
158 the interior ocean. The ice-ocean seasonal energetic cycle is computed over 300 years, using
159 climatological solar, latent and sensible heat fluxes and increasing downwelling long-wave
160 radiation, to represent the greenhouse effect. Ice retreat and freeze-up dates are diagnosed from
161 model outputs (see Appendix A for details).

162



163 **3. Link between earlier ice retreat and later freeze-up in observations and models**

164 **3.1 Trends in freeze-up and retreat date in observations and models**

165 Over 1980-2015, the ice-free season duration has increased by 9.9 ± 10.6 days / decade, with
166 nearly equal contributions of earlier ice retreat (-4.8 ± 7.7 days / decade) and later freeze-up ($4.9 \pm$
167 5.8 days /decade, median based on satellite observation, updated figures, see Table S1). Variability
168 is high however, and trends are generally not significant, except over a relatively small fraction (22%)
169 of the seasonal ice zone (Fig. 3), independently of the details of the computation (Tab. S1). The
170 patterns of changes are regionally contrasted, and Chukchi Sea is the most notable exception to the
171 rule, where later freeze-up clearly dominates changes in the ice-free season (Serreze et al., 2016, Fig.
172 3).

173 Simulated trends by the mean of selected CMIP5 models are comparable with observations, in
174 terms of ice retreat date (-4.4 ± 3.5 days / decade), freeze-up date (5.9 ± 3.3 days / decade) and ice-
175 free season duration (10.3 ± 6.3 days / decade) (Fig. 3). Individual models show larger errors, to be
176 related with mean state issues, as illustrated by the NEMO-LIM 3.6 run, for which trends in ice
177 seasonality diagnostics are in closer agreement with observations than any ESM simulation (Fig. S2).
178 One common location where trends are underestimated is the North Atlantic region, in particular
179 Barents Sea, which arguably reflects a weak meridional oceanic heat supply due to generally low
180 resolution in CMIP5 ESMs.

181

182 **3.2 Earlier sea ice retreat implies later freeze-up**

183 In terms of mean state and contemporary trends, models seem realistic enough for an analysis
184 of changes at pan-Arctic scales, but might be less meaningful at regional scales. We first study the
185 contemporary link between earlier retreat and freeze-up by looking at the sign of R 's in contemporary
186 observations and models. Because $R_{f/r}^{long}$ is a ratio of significant trends, and because all models have



187 regional differences as to where trends are significant, we base our analysis on individual models, in
188 particular IPSL-CM5A-LR.

189 Based on observations (Fig. 4), we find positive values of $R_{f/r}^{long}$ in more than 99% of grid points
190 in the studied zone, provided that computations are restricted where trends on retreat and freeze-up
191 dates are significant at a 95% level (N=5257). $R_{f/r}^{short}$ (Fig. 5) is generally smaller (0.21 ± 0.27) than
192 $R_{f/r}^{long}$ (0.71 ± 0.42 , 95% confidence level), and also positive in most pixels (87% of 23475 pixels).

193 CMIP5 models are thus consistent with the robust link between earlier ice retreat and later
194 freeze-up dates found in observations (Stammerjohn et al., 2012; Stroeve et al., 2016). More
195 generally, we find a robust link between earlier retreat and later freeze-up in all cases: both $R_{f/r}$'s are
196 virtually always positive for short and long-term computations, from observations (Fig. 4, 5) and
197 models (Fig. S3, S4), over the three analysed periods (1980-2015 for observations and models, 2015-
198 2050 and 2050-2085 for models only). This finding expands previous findings from satellite
199 observations using de-trended time series (Stammerjohn et al., 2012; Serreze et al, 2016; Stern and
200 Laidre, 2016), in particular the clear linear correlation found between de-trended ice retreat and
201 freeze-up dates (Stroeve et al., 2016). Following these authors, we attribute the strong earlier retreat
202 / later freeze-up relationship as a manifestation of the ice-albedo feedback: earlier ice retreat leads to
203 an extra absorption of heat by the upper ocean. This heat must be released back to the atmosphere
204 before the ice can start freezing again, leading to later freeze-up. This explanation is also supported
205 by satellite SST analysis in the ice-free season (Steele et al., 2008; Steele and Dickinson, 2016).
206



207 3.3 Increasingly late freeze-up dominates future changes in open water season

208 We now focus on the respective contribution of changes in retreat and freeze-up dates to the
209 increasingly long open water season, by analysing the magnitude of $R_{f/r}^{long}$. Contemporary values of
210 $R_{f/r}^{long}$ match between model and observations but not spatially (Fig. 4a,b and S3). Over 1980-2015
211 the simulated $R_{f/r}^{long}$ is slightly higher (1.1 ± 0.7) than the observational value (0.7 ± 0.4). Since models
212 never position the sea ice edge exactly, it is not surprising that the spatial distribution and the modal
213 $R_{f/r}^{long}$ differs among models and between models and observations. Indeed, the NEMO-LIM3.6 run
214 better simulates the spatial distribution of $R_{f/r}^{long}$ (see Fig. S5), which underlines the role of mean state
215 errors.

216 As far as future changes are concerned, all models show a qualitatively similar evolution (Fig.
217 1 and S6). Projected changes in ice retreat and freeze-up dates start by approximately 2000, and
218 continue at a nearly constant pace from 2040 until 2200. By 2040, the trend in freeze-up date typically
219 becomes larger than the trend in ice retreat date, as indicated by the corresponding mean $R_{f/r}^{long} = 1.8$
220 ± 0.4 over 2000-2200 (Table 1).

221 To further understand these contrasting trends between ice retreat and freeze-up dates, we
222 mapped $R_{f/r}^{long}$, over 2015-2050 and 2050-2085. We find that, in the course of the 21st century, trends
223 in retreat and freeze-up date become significant over increasingly wide regions. The overall $R_{f/r}^{long}$
224 value increases, as illustrated in Fig. 4 for the IPSL-CM5A-LR model. This behaviour is found
225 independent of the considered model (Fig. S3).

226 This finding expands the recent analyses of the CESM Large-Ensemble project (Barnhart et al.,
227 2016); and of Alaskan Arctic sea ice in CMIP5 models, finding faster ice coverage decrease in fall
228 than in spring (Wang and Overland, 2015). Both studies propose that the extra heat uptake in the
229 surface ocean due to an increased open water season as a potential explanation. As we suggested



230 earlier, this indeed explains why $R_{f/r}^{long}$ would be positive but does not explain the amplified delay in
231 freeze-up date, or why $R_{f/r}^{long}$ would be > 1 .

232

233 **3.4 A thermodynamic mechanism for an amplified delay in freeze-up date**

234 The reason why $R_{f/r}^{long}$ becomes > 1 by 2040 is related to the asymmetric response of ice-ocean
235 thermodynamics to warming. Such response emerges from simulations with a 1D thermodynamic
236 model of sea ice growth and melt in relation with the upper ocean energy budget (Semtner, 1976).
237 Without any particular tuning, the 1D model simulations feature an evolution that is similar to the
238 long-term behaviour of CMIP5 models (Fig. 1b), with trends in freeze-up date (6.0 days/decade)
239 larger than in retreat date (-3.1 days/decade), with a corresponding value of $R_{f/r}^{long} = 1.9$, all numbers
240 falling within the CMIP5 envelope (Tab. 1).

241 The link between ice retreat and freeze-up dates is in direct relation with the upper ocean energy
242 budget and the evolution of SST, in a way that goes beyond the classical ice-albedo feedback
243 explanation. After ice retreat, the SST rapidly increases due to solar absorption into the mixed layer
244 and then decreases much slower until freezing, due to non-solar ocean-to-atmosphere fluxes (Fig.
245 6a), an evolution that is similar to a recent satellite-based analysis (Steele and Dickinson, 2016).

246 In the 1D model framework, a simple expression linking $R_{f/r}^{long}$ and the ice-free ocean heat
247 fluxes can be derived (see Appendix A)

$$248 \quad R_{f/r}^{long} = Q_+/Q_-,$$

249 where Q_+ and Q_- are the absolute values of average net positive (negative) atmosphere-to-ocean heat
250 fluxes during the ice free-period. Q_+ mostly corresponds to net solar flux, typically 150 W/m^2 ,
251 whereas Q_- corresponds to the net non-solar, mostly long-wave heat flux, at freezing temperatures,
252 typically $75\text{-}150 \text{ W/m}^2$ (See Appendix B). Since $Q_+ \geq Q_-$, $R_{f/r}^{long} \geq 1$ and hence the delay in freeze-
253 up date is larger than the delay in retreat date.



254 Why $R_{f/r}^{long}$ would vary so little among CMIP5 models and even the 1D model is because
255 celestial mechanics, ubiquitous clouds and near-freezing temperatures provide strong constraints on
256 the surface radiation balance, that all models likely capture. In IPSL-CM5A-LR, the sole model for
257 which we could retrieve daily SST (Fig. 6b), the evolution of the summer SST in seasonally ice-free
258 regions features a rapid initial increase followed by slow decrease, an indication that the mechanism
259 we propose is sensible.

260

261 3.5 Inter-annual variability and extra processes add to the purely thermodynamic response

262 $R_{f/r}^{long} > 1$ only clearly emerges by 2040 in CMIP5 models, whereas $R_{f/r}^{long}$ is typically < 1 over
263 the recent past (1980-2015) from the satellite record (Fig. 4a). There are physical arguments in favour
264 of a progressive emergence of a 1D response in the course of this century. (i) The contribution of the
265 sub-surface ocean to the surface energy budget, neglected in the 1D approach, is likely larger today
266 than in the future Arctic. Over the 21st century, the Arctic stratification increases in CMIP5 models
267 (Vancoppenolle et al., 2013; Steiner et al., 2014), whereas the oceanic heat flux convergence should
268 decrease (Bitz et al., 2005). (ii) It seems also clear that the solar contribution to the upper ocean energy
269 budget is smaller today than in the future, as the date of retreat falls closer to the summer solstice.
270 (iii) The surface energy budget is less spatially coherent today than in the future, when the seasonal
271 ice zone moves northwards. The solar radiation maximum drastically changes over 45 to 65°N, but
272 has small spatial variations above the Arctic circle (Peixoto and Oort, 1992). In some specific regions,
273 $R_{f/r}^{long}$ is already > 1 , in particular in Chukchi Sea, but this is associated to the summer oceanic heat
274 transport through Bering Strait (Serreze et al., 2016), which is not the generic behaviour we see in
275 CMIP5.

276 The aforementioned processes, ignored in the 1-D model may explain why $R_{f/r}^{long} > 1$ would
277 emerge by mid-century, but inter-annual variability, also absent in the 1-D model, should also be
278 considered (Barnhart et al., 2016). It is remarkable that $R_{f/r}^{short}$ is < 1 both from satellite records (Fig.



279 5a) and from CMIP5 model simulations, for all periods and models considered (Fig. 5b-d, S4). This
280 suggests that the freeze-up amplification mechanism is not dominant at inter-annual time scales.
281 Indeed, based on inter-annual satellite time series, the standard deviation of ice retreat (STD=21.6
282 days) and freeze-up dates (STD=14.3 days) is high (Stroeve et al., 2016) and the corresponding trends
283 over 1980-2015 are not significant. Conceivably, atmosphere, ocean and ice horizontal transport,
284 operating at synoptic to inter-annual time scales, obscure the simple thermodynamic relation between
285 the ice retreat and freeze-up dates found in the 1D model. Altogether, this highlights that the freeze-
286 up amplification mechanism is a long-term process, and stress the importance of the considered time
287 scales and period as previous studies have already shown (Parkinson et al., 2014; Barnhart et al.,
288 2016).
289



290 **4. Conclusions**

291 The present analysis, focused on contemporary and future changes in sea ice seasonality, based
292 on satellite retrievals and Earth System Model simulations of ice coverage, raised the following key
293 findings:

294 1. The 1980-2015 long-term trends in ice retreat and freeze-up dates are of similar magnitude
295 but still insignificant over 78% of the seasonal ice zone.

296 2. CMIP5 models consistently project a long-term rate of change in freeze-up date that is about
297 twice as large as the rate of change in ice retreat date: the open water season shifts into fall.

298 3. The reduced surface albedo and the enhanced solar radiation uptake by the ocean had
299 previously been put forward to explain such changes in sea ice seasonality. Next to these two
300 elements, our analysis highlights a third, new element: the comparatively slow heat loss by ice-free
301 waters before freeze-up, which is the key contributor to the amplified delay in freeze-up date.

302 More generally, thermodynamic processes exert a central control on sea ice seasonality. The
303 ice-albedo feedback provides a strong link between earlier ice retreat and later freeze-up, a link that
304 is found in both satellite retrievals and climate projections, regardless of the considered period and
305 time scale, expanding findings from previous works (Stammerjohn et al., 2012; Serreze et al, 2016;
306 Stern and Laidre, 2016; Stroeve et al., 2016). Why long-term trends in freeze up date are ultimately
307 about twice as large as the trends in ice retreat date is also of thermodynamic origin: extra solar heat
308 reaching the ocean due to earlier ice retreat is absorbed at a higher rate than it can be released until
309 freeze-up. The long-term response to warming of ice seasonality, turns up by mid-century in CMIP5
310 simulations, when changes in the ice-free season emerge out of variability (Barnhart et al., 2016).
311 Variability seems essentially driven by dynamical processes, a setup that has other analogs in climate
312 change studies (Bony et al., 2004; Kröner et al., 2017; Shepherd, 2014). The suggested increase in
313 the ice-free season and shift into fall are part of broader seasonal changes in the climate system.
314 Global warming induces changes in the seasonal cycle of surface temperature (Thomson, 1995), both



315 in terms of amplitude and phase (Dwyer et al., 2012), in relation with the surface energy fluxes and
316 the presence of sea ice (Dwyer et al., 2012; Donohoe and Battisti, 2013).

317 As the Arctic sea ice seasonality is a basic trait of the Arctic Ocean, a shift of the Arctic sea
318 ice-free season would also have direct ecosystem and socio-economic impacts. The length of the
319 Arctic sea ice season exerts a first-order control on the light reaching phytoplankton (Arrigo and van
320 Dijken, 2011; Wassmann and Reigstad, 2011, Assmy et al., 2017) and is crucial to some marine
321 mammals, such as walrus (Laidre et al., 2015) and polar bears (Stern and Laidre, 2016), who use
322 sea ice as a living platform. The shift in the sea ice seasonal cycle will progressively break the close
323 association between the ice-free season and the seasonal photoperiod in Arctic waters, a relation that
324 is fundamental to photosynthetic marine organisms existing in present climate (Arrigo and van
325 Dijken, 2011). Indeed, because the freeze-up date is projected to overtake the onset of polar night
326 (Fig. 1), typically by 2050, changes in the photoperiod are at this point solely determined by the ice
327 retreat date, and no more by freeze-up date. The duration of the sea ice season also affects travel and
328 hunting habits of coastal human communities (Huntington et al, 2017) and restricts the shipping
329 season (Smith and Stephenson, 2013; Melia et al., 2017). The second clear implication of the foreseen
330 shift of the Arctic open water season is that the Arctic navigability would expand to fall, well beyond
331 the onset of polar night, supporting the lengthening of the shipping season mostly by later closing
332 dates (Melia et al., 2017).

333 Better projecting future changes in sea ice and its seasonality is fundamental to our
334 understanding of the future Arctic Ocean. Pinpointing the drivers of sea ice seasonality, in particular
335 the upper ocean energy budget (Donohoe and Battisti, 2013) as well as understanding the impact of
336 better resolved ocean currents are critical to reduce uncertainties. Further knowledge can be acquired
337 from observations (e.g. Steele and Dickinson, 2016) and Earth System Model analyses, for which the
338 expanded set of ice-ocean diagnostics expected in CMIP6 (Notz et al., 2016) will prove instrumental.



339 **Code, data and sample availability**

340 Scripts available upon request.

341 Contact: Marion Lebrun, Laboratoire d'Océanographie et du Climat, IPSL Boite 100, 4 Place

342 Jussieu, 75252 Paris CEDEX 05, France.



343 **Appendices**

344 **Appendix A: Upper ocean energetics and ice seasonality in the 1D ice-ocean model**

345 We use the Semtner (1976) zero-layer approach for ice growth and melt above an upper oceanic
346 layer taking up heat. Snow is neglected. The ice model equations for surface temperature (T_{su}) and
347 ice thickness (h) read:

$$348 \quad Q_{atm}(T_{su}) = Q_c(T_{su}), \quad (1)$$

$$349 \quad \rho L \frac{dh}{dt} = Q_{atm}(T_{su}) + Q_w. \quad (2)$$

350 where $Q_{atm} = Q_0 + Q_{sol}(1 - \alpha_i) - \epsilon\sigma T_{su}^4$, with Q_0 the sum of downwelling long-wave, latent and
351 sensible heat fluxes, Q_{sol} the incoming solar flux, $\alpha_i = 0.64$ the ice albedo, $\epsilon = 0.98$ the emissivity
352 and $\sigma = 5.67 \times 10^{-8} W/m^2/K^4$ the Stefan-Boltzmann constant. Q_c is the heat conduction flux in
353 the ice (> 0 downwards), Q_w is the ocean-to-ice sensible heat flux at the ice base, $\rho = 900 kg/m^3$
354 is ice density and $L = 334 kJ/kg$ is the latent heat of fusion. Once the ice thickness vanishes, the
355 water temperature T_w in a $h_w = 30m$ -thick upper ocean layer follows:

$$356 \quad \rho_w c_w \frac{\partial T_w}{\partial t} h_w = Q_0 + Q_{sol}(1 - \alpha_w)[1 - \exp(-\kappa h_w)] - \epsilon\sigma T_w^4. \quad (3)$$

357 $\rho_w = 1025 kg/m^3$ is water density, $c_w = 4000 J/kg/K$ is water specific heat, $\kappa_w = 1/30 m^{-1}$ is
358 the solar radiation attenuation coefficient in water. Ice starts forming back once T_w returns to the
359 freezing point $T_f = -1.8^\circ C$.

360 The atmospheric solar (Q_{sol}) and non-solar (Q_0) heat fluxes are forced using the classical standard
361 monthly mean climatologies, typical of Central Arctic conditions (Fletcher, 1965). We add an extra
362 $Q_{nsol} = 0.1 W/m^2$ to the non-solar flux each year to simulate the greenhouse effect. We impose
363 $Q_w = 2 W/m^2$ following Maykut and Untersteiner (1971). Ice becomes seasonal after 127 years.
364 The model is run until there is no ice left, which takes 324 years.

365 The following three diagnostics are used to describe the ice-ocean seasonality (see Fig. 1):



366 • d_r (ice retreat date): the first day with $T_w > T_f = -1.8^\circ\text{C}$;

367 • d_f (ice freeze-up date): the last day with $T_w > T_f = -1.8^\circ\text{C}$;

368 • d_{max} (maximum water temperature date): the last day with $Q > 0$.

369 Let us now detail how the ratio of ice freeze-up and retreat dates trends $R_{f/r}^{long}$ is related to the
 370 energy budget of the ice-free ocean in the 1-D model. We first express the relation between ice
 371 freeze-up and ice retreat dates for a given year. Since heat fluxes are strongly constrained by the
 372 imposed forcing, the freeze-up date d_f is directly connected with d_r . Once ice has disappeared on
 373 $d = d_r$, the upper ocean takes up energy and warms from the freezing point until T_w is
 374 maximum on $d = d_{max}$. Then the upper ocean loses energy until T_w returns to the freezing point
 375 ($d = d_f$). Over this temperature path, the energy gain from d_f to d_{max} must equal the energy loss
 376 from d_{max} to d_f , which can be written as:

$$377 \quad Q_+(d_{max} - d_r) = -Q_-(d_f - d_{max}), \quad (4)$$

378 where $Q_+ (> 0)$ is defined as the average net heat flux to the upper ocean over $[d_r, d_{max}]$ and $Q_- (<$
 379 $0)$ is the average net heat flux over $[d_{max}, d_f]$. Referring d_r and d_f with respect to d_{max} :

$$380 \quad d'_r = d_r - d_{max}, \quad (5)$$

$$381 \quad d'_f = d_f - d_{max}, \quad (6)$$

382 and defining the ice-free ocean energetic ratio as $R_Q \equiv Q_+/Q_-$, Eq. (4) simplifies into:

$$383 \quad d'_f = R_Q d'_r. \quad (7)$$

384 In other words, the time difference between freeze-up date and upper ocean temperature maximum
 385 is R_Q times the difference between the dates of maximum water temperature and ice retreat. In
 386 practice, Q_+ is always higher than Q_- , hence R_Q is always >1 , i.e., the heat enters into the upper



387 ocean faster than it escapes, T_w increases faster than it decreases and $d'_f > d'_r$. Note that the relation
 388 (7) is not valid in reality because of ice dynamics and other three-dimensional processes.

389 We now seek to express the change in freeze-up date Δd_f as a function of the change in ice retreat
 390 date Δd_r , over two different years (labelled with subscripts 1 and 2), because of a change in
 391 atmospheric forcing. Using d_{max} as the origin of time, Δd_r and Δd_f can be expressed as:

$$392 \quad \Delta d_r = d'_{r,2} - d'_{r,1} - \Delta d_{max}, \quad (8)$$

$$393 \quad \Delta d_f = d'_{f,2} - d'_{f,1} - \Delta d_{max}. \quad (9)$$

394 Multiplying Eq. (8) by $R_{Q,2}$, then using Eq. (7) in Eq. (8) to substitute $d'_{r,1} = d'_{f,1}/R_{Q,1}$ and in Eq.
 395 (9) to substitute $d'_{f,2} = R_{Q,2}d'_{r,2}$, then subtracting Eq. (9) from Eq. (8), and finally rearranging
 396 terms, one retrieves the shift in freeze-up date:

$$397 \quad \Delta d_f = R_{Q,2}\Delta d_r + \left(\frac{R_{Q,2}}{R_{Q,1}} - 1\right)d'_{f,1} + (1 - R_{Q,2})\Delta d_{max}, \quad (10)$$

398 which is an exact solution (see Fig. A1). A good approximation to this can be found by assuming
 399 that years 1 and 2 are not too far in time, $R_2 \approx R_1$ and $\Delta d_{max} \approx 0$, hence the last two terms drop
 400 and the shift in freeze-up date further simplifies into:

$$401 \quad \Delta d_f \approx R_{Q,2}\Delta d_r = \frac{Q_{+2}}{Q_{-2}}\Delta d_r. \quad (11)$$

402 The shift in freeze-up date is thus nearly equal to the shift in ice retreat date multiplied by the
 403 Q_+/Q_- ratio and is therefore always higher than Δd_r . This last equation provides a concise and
 404 powerful simplification of the energetics of the system under consideration. It states that, in the
 405 Semtner (1976) zero-layer one-dimensional idealised ice-ocean system, the response of the
 406 seasonality of the ice cover to changes in atmospheric forcing can be directly estimated from the
 407 surface energy balance of the ice-free ocean.

408



409 **Appendix B: scaling of the ice-free ocean energy budget**

410 1D model results show a direct link between, on the one hand, the ratio of long-term trends in
411 freeze-up and ice retreat date ($R_{f/r}^{long}$), and the energetics of the ice-free ocean on the other hand:

$$412 \quad R_{f/r}^{long} = Q_+/Q_-,$$

413 where Q_+ and Q_- are the absolute values of average net positive (negative) atmosphere-to-ocean
414 heat fluxes during the ice free-period. CMIP6 and 1D model results suggest that over long-time
415 scales, this ratio is stable and does not vary much among models, with values ranging from 1.5 to 2.
416 Why this ratio would be so invariable is because celestial mechanics, ubiquitous clouds and near-
417 freezing temperatures provide strong constraints on the radiation balance, which dominates the
418 surface energy budget.

419 Assuming that non-solar components cancel each other, the mean heat gain is mostly solar:

$$420 \quad Q_+ = \langle Q_{sol}(1 - \alpha_w)[1 - \exp(-\kappa h_w)] \rangle |_{early\ ice-free\ season},$$

421 where the mean is taken over the first part of the ice-free period, typically covering July or June. Of
422 remarkable importance is that the magnitude of clear-sky solar flux above the Arctic Circle deviates
423 by less than 20 W/m², both in space and time, around the summer solstice (see, e.g., Peixoto and
424 Oort, 1992). Assuming summer cloud skies would remain the norm, we take 150 W/m² as
425 representative for Q_+ .

426 The mean heat loss is mostly non-solar:

$$427 \quad Q_- = -\langle Q_{lw} - \epsilon\sigma T_w^4 + Q_{sh} + Q_{lh} \rangle |_{late\ ice-free\ season},$$

428 and corresponds to the second part of the ice-free period, typically covering September and
429 October. Downwelling long-wave radiation flux Q_{lw} corresponds to cloud skies at near freezing
430 temperatures, for which 250 W/m² seems reasonable (Persson et al., 2002). The thermal emission



431 would be that of the ocean, a nearly ideal black body, at near-freezing temperatures, and should not
432 depart much from 300 W/m^2 . The sensible (Q_{sh}) and latent (Q_{lh}) heat fluxes are relatively more
433 uncertain. In current ice-covered conditions, turbulent fluxes imply a net average heat loss, typically
434 smaller than 10 W/m^2 (Personn et al., 2002). Over an ice-free ocean however, turbulent heat losses
435 would obviously increase, in particular through the latent heat flux, but also become more variable
436 at synoptic time scales. Assuming that turbulent heat fluxes would in the future Arctic compare to
437 what they are today in ice-free ocean regions of the North Pacific, we argue that they would
438 correspond to a 25 W/m^2 heat loss, definitely not exceeding 100 W/m^2 (Yu et al., 2008).

439 Taken together, these elements give an estimated R value ranging from 1 to 2, where uncertainties
440 on the dominant radiation terms of the energy budget are small and inter-model differences in
441 turbulent heat fluxes would be decisive in determining the actual value of the ratio.

442



443 **Author Contribution**

444 All authors conceived the study and co-wrote the paper. ML and MV performed analyses.

445

446 **Competing contribution**

447 The authors declare that they have no conflict of interest.



448 **References**

- 449 Arrigo, K. R. and van Dijken, G. L.: Secular trends in Arctic Ocean net primary production, J.
450 Geophys. Res., 116(C9), C09011, doi:[10.1029/2011JC007151](https://doi.org/10.1029/2011JC007151), 2011.
- 451 Assmy, P., Fernández-Méndez, M., Duarte, P., Meyer, A., Randelhoff, A., Mundy, C. J., Olsen, L.
452 M., Kauko, H. M., Bailey, A., Chierici, M., Cohen, L., Doulgeris, A. P., Ehn, J. K., Fransson, A.,
453 Gerland, S., Hop, H., Hudson, S. R., Hughes, N., Itkin, P., Johnsen, G., King, J. A., Koch, B. P.,
454 Koenig, Z., Kwasniewski, S., Laney, S. R., Nicolaus, M., Pavlov, A. K., Polashenski, C. M.,
455 Provost, C., Rösel, A., Sandbu, M., Spreen, G., Smedsrud, L. H., Sundfjord, A., Taskjelle, T.,
456 Tatarek, A., Wiktor, J., Wagner, P. M., Wold, A., Steen, H. and Granskog, M. A.: Leads in Arctic
457 pack ice enable early phytoplankton blooms below snow-covered sea ice, Scientific Reports, 7,
458 [srep40850](https://doi.org/10.1038/srep40850), doi:[10.1038/srep40850](https://doi.org/10.1038/srep40850), 2017.
- 459 Barnhart, K. R., Miller, C. R., Overeem, I. and Kay, J. E.: Mapping the future expansion of Arctic
460 open water, Nature Clim. Change, 6(3), 280–285, doi:[10.1038/nclimate2848](https://doi.org/10.1038/nclimate2848), 2016.
- 461 Bitz, C. M., Holland, M. M., Hunke, E. C. and Moritz, R. E.: Maintenance of the Sea-Ice Edge, J.
462 Climate, 18(15), 2903–2921, doi:[10.1175/JCLI3428.1](https://doi.org/10.1175/JCLI3428.1), 2005.
- 463 Blanchard-Wrigglesworth, E., Armour, K. C., Bitz, C. M. and DeWeaver, E.: Persistence and
464 Inherent Predictability of Arctic Sea Ice in a GCM Ensemble and Observations, J. Climate, 24(1),
465 231–250, doi:[10.1175/2010JCLI3775.1](https://doi.org/10.1175/2010JCLI3775.1), 2010.
- 466 Bony, S., Dufresne, J.-L., Treut, H. L., Morcrette, J.-J. and Senior, C.: On dynamic and
467 thermodynamic components of cloud changes, Climate Dynamics, 22(2–3), 71–86,
468 doi:[10.1007/s00382-003-0369-6](https://doi.org/10.1007/s00382-003-0369-6), 2004.
- 469 Cavalieri, D. J. and Parkinson, C. L.: Arctic sea ice variability and trends, 1979–2010, The
470 Cryosphere, 6(4), 881–889, doi:[10.5194/tc-6-881-2012](https://doi.org/10.5194/tc-6-881-2012), 2012.



- 471 Collins, W. J., Bellouin, N., Doutriaux-Boucher, M., Gedney, N., Halloran, P., Hinton, T., Hughes,
472 J., Jones, C. D., Joshi, M., Liddicoat, S., Martin, G., O'Connor, F., Rae, J., Senior, C., Sitch, S.,
473 Totterdell, I., Wiltshire, A. and Woodward, S.: Development and evaluation of an Earth-System
474 model – HadGEM2, *Geosci. Model Dev.*, 4(4), 1051–1075, doi:[10.5194/gmd-4-1051-2011](https://doi.org/10.5194/gmd-4-1051-2011), 2011.
- 475 Comiso, Josephino `Joey`: Bootstrap Sea Ice Concentrations from Nimbus-7 SMMR and DMSP
476 SSM/I-SSMIS, Version 2, , doi:[10.5067/J6JQLS9EJ5HU](https://doi.org/10.5067/J6JQLS9EJ5HU), 2000.
- 477 Donohoe, A. and Battisti, D. S.: The Seasonal Cycle of Atmospheric Heating and Temperature, *J.*
478 *Climate*, 26(14), 4962–4980, doi:[10.1175/JCLI-D-12-00713.1](https://doi.org/10.1175/JCLI-D-12-00713.1), 2013.
- 479 Dufresne, J.-L., Foujols, M.-A., Denvil, S., Caubel, A., Marti, O., Aumont, O., Balkanski, Y.,
480 Bekki, S., Bellenger, H., Benschila, R., Bony, S., Bopp, L., Braconnot, P., Brockmann, P., Cadule,
481 P., Cheruy, F., Codron, F., Cozic, A., Cugnet, D., Noblet, N. de, Duvel, J.-P., Ethé, C., Fairhead, L.,
482 Fichet, T., Flavoni, S., Friedlingstein, P., Grandpeix, J.-Y., Guez, L., Guilyardi, E., Hauglustaine,
483 D., Hourdin, F., Idelkadi, A., Ghattas, J., Joussaume, S., Kageyama, M., Krinner, G., Labetoulle, S.,
484 Lahellec, A., Lefebvre, M.-P., Lefevre, F., Levy, C., Li, Z. X., Lloyd, J., Lott, F., Madec, G.,
485 Mancip, M., Marchand, M., Masson, S., Meurdesoif, Y., Mignot, J., Musat, I., Parouty, S., Polcher,
486 J., Rio, C., Schulz, M., Swingedouw, D., Szopa, S., Talandier, C., Terray, P., Viovy, N. and
487 Vuichard, N.: Climate change projections using the IPSL-CM5 Earth System Model: from CMIP3
488 to CMIP5, *Clim Dyn*, 40(9–10), 2123–2165, doi:[10.1007/s00382-012-1636-1](https://doi.org/10.1007/s00382-012-1636-1), 2013.
- 489 Dussin, R., B. Barnier and L. Brodeau, *The making of Drakkar forcing set DFS5*. Tech. report
490 DRAKKAR/MyOcean Report 01-04-16, LGGE, Grenoble, France. (2016).
- 491 Dwyer, J. G., Biasutti, M. and Sobel, A. H.: Projected Changes in the Seasonal Cycle of Surface
492 Temperature, *J. Climate*, 25(18), 6359–6374, doi:[10.1175/JCLI-D-11-00741.1](https://doi.org/10.1175/JCLI-D-11-00741.1), 2012.
- 493 Fletcher, J. O., The heat budget of the Arctic Basin and its relation to climate, Rep. R-444-PR,
494 RAND Corp., Santa Monica, Calif., (1965).



495 Gent, P. R., Danabasoglu, G., Donner, L. J., Holland, M. M., Hunke, E. C., Jayne, S. R., Lawrence,
496 D. M., Neale, R. B., Rasch, P. J., Vertenstein, M., Worley, P. H., Yang, Z.-L. and Zhang, M.: The
497 Community Climate System Model Version 4, *J. Climate*, 24(19), 4973–4991,
498 doi:[10.1175/2011JCLI4083.1](https://doi.org/10.1175/2011JCLI4083.1), 2011.

499 Giorgetta Marco A., Jungclaus Johann, Reick Christian H., Legutke Stephanie, Bader Jürgen,
500 Böttinger Michael, Brovkin Victor, Crueger Traute, Esch Monika, Fieg Kerstin, Glushak Ksenia,
501 Gayler Veronika, Haak Helmuth, Hollweg Heinz-Dieter, Ilyina Tatiana, Kinne Stefan, Kornblueh
502 Luis, Matei Daniela, Mauritsen Thorsten, Mikolajewicz Uwe, Mueller Wolfgang, Notz Dirk, Pithan
503 Felix, Raddatz Thomas, Rast Sebastian, Redler Rene, Roeckner Erich, Schmidt Hauke, Schnur
504 Reiner, Segschneider Joachim, Six Katharina D., Stockhause Martina, Timmreck Claudia, Wegner
505 Jörg, Widmann Heinrich, Wieners Karl-H., Claussen Martin, Marotzke Jochem and Stevens Bjorn:
506 Climate and carbon cycle changes from 1850 to 2100 in MPI-ESM simulations for the Coupled
507 Model Intercomparison Project phase 5, *Journal of Advances in Modeling Earth Systems*, 5(3),
508 572–597, doi:[10.1002/jame.20038](https://doi.org/10.1002/jame.20038), 2013.

509 Hezel, P. J., Fichet, T. and Massonnet, F.: Modeled Arctic sea ice evolution through 2300 in
510 CMIP5 extended RCPs, *The Cryosphere*, 8(4), 1195–1204, doi:[10.5194/tc-8-1195-2014](https://doi.org/10.5194/tc-8-1195-2014), 2014.

511 Huntington, H. P., Gearheard, S., Holm, L. K., Noongwook, G., Opie, M. and Sanguya, J.: Sea ice
512 is our beautiful garden: indigenous perspectives on sea ice in the Arctic, in *Sea Ice*, edited by D. N.
513 Thomas, pp. 583–599, John Wiley & Sons, Ltd., 2017.

514 Johnson, M. and Eicken, H.: Estimating Arctic sea-ice freeze-up and break-up from the satellite
515 record: A comparison of different approaches in the Chukchi and Beaufort Seas, *Elem Sci Anth*,
516 4(0), doi:[10.12952/journal.elementa.000124](https://doi.org/10.12952/journal.elementa.000124), 2016.



- 517 Kröner, N., Kotlarski, S., Fischer, E., Lüthi, D., Zubler, E. and Schär, C.: Separating climate change
518 signals into thermodynamic, lapse-rate and circulation effects: theory and application to the
519 European summer climate, *Clim Dyn*, 48(9–10), 3425–3440, doi:[10.1007/s00382-016-3276-3](https://doi.org/10.1007/s00382-016-3276-3),
520 2017.
- 521 Kwok, R. and Rothrock, D. A.: Decline in Arctic sea ice thickness from submarine and ICESat
522 records: 1958–2008, *Geophys. Res. Lett.*, 36(15), L15501, doi:[10.1029/2009GL039035](https://doi.org/10.1029/2009GL039035), 2009.
- 523 Laidre, K. L., Stern, H., Kovacs, K. M., Lowry, L., Moore, S. E., Regehr, E. V., Ferguson, S. H.,
524 Wiig, Ø., Boveng, P., Angliss, R. P., Born, E. W., Litovka, D., Quakenbush, L., Lydersen, C.,
525 Vongraven, D. and Ugarte, F.: Arctic marine mammal population status, sea ice habitat loss, and
526 conservation recommendations for the 21st century, *Conservation Biology*, 29(3), 724–737,
527 doi:[10.1111/cobi.12474](https://doi.org/10.1111/cobi.12474), 2015.
- 528 Lindsay, R. and Schweiger, A.: Arctic sea ice thickness loss determined using subsurface, aircraft,
529 and satellite observations, *The Cryosphere*, 9(1), 269–283, doi:[10.5194/tc-9-269-2015](https://doi.org/10.5194/tc-9-269-2015), 2015.
- 530 Markus, T., Stroeve, J. C. and Miller, J.: Recent changes in Arctic sea ice melt onset, freezeup, and
531 melt season length, *J. Geophys. Res.*, 114(C12), C12024, doi:[10.1029/2009JC005436](https://doi.org/10.1029/2009JC005436), 2009.
- 532 Maslanik, J., Stroeve, J., Fowler, C. and Emery, W.: Distribution and trends in Arctic sea ice age
533 through spring 2011, *Geophys. Res. Lett.*, 38(13), L13502, doi:[10.1029/2011GL047735](https://doi.org/10.1029/2011GL047735), 2011.
- 534 Massonnet, F., Fichefet, T., Goosse, H., Bitz, C. M., Philippon-Berthier, G., Holland, M. M. and
535 Barriat, P.-Y.: Constraining projections of summer Arctic sea ice, *The Cryosphere*, 6(6), 1383–
536 1394, doi:[10.5194/tc-6-1383-2012](https://doi.org/10.5194/tc-6-1383-2012), 2012.
- 537 Maykut, G. A. and Untersteiner, N.: Some results from a time-dependent thermodynamic model of
538 sea ice, *J. Geophys. Res.*, 76(6), 1550–1575, doi:[10.1029/JC076i006p01550](https://doi.org/10.1029/JC076i006p01550), 1971.
- 539 Melia, N., Haines, K., Hawkins, E. and Day, J. J.: Towards seasonal Arctic shipping route
540 predictions, *Environ. Res. Lett.*, 12(8), 084005, doi:[10.1088/1748-9326/aa7a60](https://doi.org/10.1088/1748-9326/aa7a60), 2017.



- 541 Notz, D., Jahn, A., Holland, M., Hunke, E., Massonnet, F., Stroeve, J., Tremblay, B. and
542 Vancoppenolle, M.: The CMIP6 Sea-Ice Model Intercomparison Project (SIMIP): understanding
543 sea ice through climate-model simulations, *Geosci. Model Dev.*, 9(9), 3427–3446,
544 doi:[10.5194/gmd-9-3427-2016](https://doi.org/10.5194/gmd-9-3427-2016), 2016.
- 545 Notz, D. and Stroeve, J.: Observed Arctic sea-ice loss directly follows anthropogenic CO₂
546 emission, *Science*, aag2345, doi:[10.1126/science.aag2345](https://doi.org/10.1126/science.aag2345), 2016.
- 547 Parkinson, C. L.: Spatial patterns in the length of the sea ice season in the Southern Ocean, 1979–
548 1986, *J. Geophys. Res.*, 99(C8), 16327–16339, doi:[10.1029/94JC01146](https://doi.org/10.1029/94JC01146), 1994.
- 549 Parkinson, C. L.: Global Sea Ice Coverage from Satellite Data: Annual Cycle and 35-Yr Trends, *J.*
550 *Climate*, 27(24), 9377–9382, doi:[10.1175/JCLI-D-14-00605.1](https://doi.org/10.1175/JCLI-D-14-00605.1), 2014.
- 551 Peixoto, J. P. and Oort, A. H.: *Physics of Climate*, 1992 ed., American Institute of Physics, New
552 York., 1992.
- 553 Perovich, D. K., Light, B., Eicken, H., Jones, K. F., Runciman, K. and Nghiem, S. V.: Increasing
554 solar heating of the Arctic Ocean and adjacent seas, 1979–2005: Attribution and role in the ice-
555 albedo feedback, *Geophys. Res. Lett.*, 34(19), L19505, doi:[10.1029/2007GL031480](https://doi.org/10.1029/2007GL031480), 2007.
- 556 Persson, P. O. G., Fairall, C. W., Andreas, E. L., Guest, P. S. and Perovich, D. K.: Measurements
557 near the Atmospheric Surface Flux Group tower at SHEBA: Near-surface conditions and surface
558 energy budget, *Journal of Geophysical Research (Oceans)*, 107, 8045, doi:[10.1029/2000JC000705](https://doi.org/10.1029/2000JC000705),
559 2002.
- 560 Renner, A. H. H., Gerland, S., Haas, C., Spreen, G., Beckers, J. F., Hansen, E., Nicolaus, M. and
561 Goodwin, H.: Evidence of Arctic sea ice thinning from direct observations, *Geophys. Res. Lett.*,
562 41(14), 5029–5036, doi:[10.1002/2014GL060369](https://doi.org/10.1002/2014GL060369), 2014.
- 563 Rotstayn, L. D., Jeffrey, S. J., Collier, M. A., Dravitzki, S. M., Hirst, A. C., Syktus, J. I. and Wong,
564 K. K.: Aerosol- and greenhouse gas-induced changes in summer rainfall and circulation in the



- 565 Australasian region: a study using single-forcing climate simulations, *Atmos. Chem. Phys.*, 12(14),
566 6377–6404, doi:[10.5194/acp-12-6377-2012](https://doi.org/10.5194/acp-12-6377-2012), 2012.
- 567 Rousset, C., Vancoppenolle, M., Madec, G., Fichet, T., Flavoni, S., Barthélemy, A., Benshila, R.,
568 Chanut, J., Levy, C., Masson, S. and Vivier, F.: The Louvain-La-Neuve sea ice model LIM3.6:
569 global and regional capabilities, *Geosci. Model Dev.*, 8(10), 2991–3005, doi:[10.5194/gmd-8-2991-](https://doi.org/10.5194/gmd-8-2991-2015)
570 [2015](https://doi.org/10.5194/gmd-8-2991-2015), 2015.
- 571 Schmidt, G. A., Kelley, M., Nazarenko, L., Ruedy, R., Russell, G. L., Aleinov, I., Bauer, M., Bauer,
572 S. E., Bhat, M. K., Bleck, R., Canuto, V., Chen, Y.-H., Cheng, Y., Clune, T. L., Del Genio, A., de
573 Fainchtein, R., Faluvegi, G., Hansen, J. E., Healy, R. J., Kiang, N. Y., Koch, D., Lacis, A. A.,
574 LeGrande, A. N., Lerner, J., Lo, K. K., Matthews, E. E., Menon, S., Miller, R. L., Oinas, V., Olosolajo,
575 A. O., Perlwitz, J. P., Puma, M. J., Putman, W. M., Rind, D., Romanou, A., Sato, M., Shindell, D.
576 T., Sun, S., Syed, R. A., Tausnev, N., Tsigaridis, K., Unger, N., Voulgarakis, A., Yao, M.-S. and
577 Zhang, J.: Configuration and assessment of the GISS ModelE2 contributions to the CMIP5 archive,
578 *J. Adv. Model. Earth Syst.*, 6(1), 141–184, doi:[10.1002/2013MS000265](https://doi.org/10.1002/2013MS000265), 2014.
- 579 Semtner, A. J.: A Model for the Thermodynamic Growth of Sea Ice in Numerical Investigations of
580 Climate, *J. Phys. Oceanogr.*, 6(3), 379–389, doi:[10.1175/1520-](https://doi.org/10.1175/1520-0485(1976)006<0379:AMFTTG>2.0.CO;2)
581 [0485\(1976\)006<0379:AMFTTG>2.0.CO;2](https://doi.org/10.1175/1520-0485(1976)006<0379:AMFTTG>2.0.CO;2), 1976.
- 582 Serreze, M. C., Crawford, A. D., Stroeve, J. C., Barrett, A. P. and Woodgate, R. A.: Variability,
583 trends, and predictability of seasonal sea ice retreat and advance in the Chukchi Sea, *J. Geophys.*
584 *Res. Oceans*, 121(10), 7308–7325, doi:[10.1002/2016JC011977](https://doi.org/10.1002/2016JC011977), 2016.
- 585 Shepherd, T. G.: Atmospheric circulation as a source of uncertainty in climate change projections,
586 *Nature Geoscience*, 7(10), 703–708, doi:[10.1038/ngeo2253](https://doi.org/10.1038/ngeo2253), 2014.
- 587 Smith, L. C. and Stephenson, S. R.: New Trans-Arctic shipping routes navigable by midcentury,
588 *PNAS*, 110(13), E1191–E1195, doi:[10.1073/pnas.1214212110](https://doi.org/10.1073/pnas.1214212110), 2013.



- 589 Stammerjohn, S., Massom, R., Rind, D. and Martinson, D.: Regions of rapid sea ice change: An
590 inter-hemispheric seasonal comparison, *Geophys. Res. Lett.*, 39(6), L06501,
591 doi:[10.1029/2012GL050874](https://doi.org/10.1029/2012GL050874), 2012.
- 592 Steele, M., Ermold, W. and Zhang, J.: Arctic Ocean surface warming trends over the past 100 years,
593 *Geophys. Res. Lett.*, 35(2), L02614, doi:[10.1029/2007GL031651](https://doi.org/10.1029/2007GL031651), 2008.
- 594 Steele, M. and Dickinson, S.: The phenology of Arctic Ocean surface warming, *J. Geophys. Res.*
595 *Oceans*, 121(9), 6847–6861, doi:[10.1002/2016JC012089](https://doi.org/10.1002/2016JC012089), 2016.
- 596 Steiner, N. S., Christian, J. R., Six, K. D., Yamamoto, A. and Yamamoto-Kawai, M.: Future ocean
597 acidification in the Canada Basin and surrounding Arctic Ocean from CMIP5 earth system models,
598 *J. Geophys. Res. Oceans*, 119(1), 332–347, doi:[10.1002/2013JC009069](https://doi.org/10.1002/2013JC009069), 2014.
- 599 Stern, H. L. and Laidre, K. L.: Sea-ice indicators of polar bear habitat, *The Cryosphere*, 10(5),
600 2027–2041, doi:[10.5194/tc-10-2027-2016](https://doi.org/10.5194/tc-10-2027-2016), 2016.
- 601 Stroeve, J. C., Kattsov, V., Barrett, A., Serreze, M., Pavlova, T., Holland, M. and Meier, W. N.:
602 Trends in Arctic sea ice extent from CMIP5, CMIP3 and observations, *Geophys. Res. Lett.*, 39(16),
603 L16502, doi:[10.1029/2012GL052676](https://doi.org/10.1029/2012GL052676), 2012.
- 604 Stroeve, J. C., Crawford, A. D. and Stammerjohn, S.: Using timing of ice retreat to predict timing of
605 fall freeze-up in the Arctic, *Geophys. Res. Lett.*, 43(12), 2016GL069314,
606 doi:[10.1002/2016GL069314](https://doi.org/10.1002/2016GL069314), 2016.
- 607 Thomson, D. J.: The seasons, global temperature, and precession, *Science*, 268(5207), 59–68,
608 doi:[10.1126/science.268.5207.59](https://doi.org/10.1126/science.268.5207.59), 1995.
- 609 Uotila, P., Iovino, D., Vancoppenolle, M., Lensu, M. and Rousset, C.: Comparing sea ice,
610 hydrography and circulation between NEMO3.6 LIM3 and LIM2, *Geosci. Model Dev.*, 10(2),
611 1009–1031, doi:[10.5194/gmd-10-1009-2017](https://doi.org/10.5194/gmd-10-1009-2017), 2017.



- 612 Vancoppenolle, M., Bopp, L., Madec, G., Dunne, J., Ilyina, T., Halloran, P. R. and Steiner, N.:
613 Future Arctic Ocean primary productivity from CMIP5 simulations: Uncertain outcome, but
614 consistent mechanisms, *Global Biogeochem. Cycles*, 27(3), 605–619, doi:[10.1002/gbc.20055](https://doi.org/10.1002/gbc.20055),
615 2013.
- 616 Voldoire, A., Sanchez-Gomez, E., Méliá, D. S. y, Decharme, B., Cassou, C., Sénési, S., Valcke, S.,
617 Beau, I., Alias, A., Chevallier, M., Déqué, M., Deshayes, J., Douville, H., Fernandez, E., Madec,
618 G., Maisonnave, E., Moine, M.-P., Planton, S., Saint-Martin, D., Szopa, S., Tyteca, S., Alkama, R.,
619 Belamari, S., Braun, A., Coquart, L. and Chauvin, F.: The CNRM-CM5.1 global climate model:
620 description and basic evaluation, *Clim Dyn*, 40(9–10), 2091–2121, doi:[10.1007/s00382-011-1259-](https://doi.org/10.1007/s00382-011-1259-y)
621 [y](https://doi.org/10.1007/s00382-011-1259-y), 2013.
- 622 Wang, M. and Overland, J. E.: Projected future duration of the sea-ice-free season in the Alaskan
623 Arctic, *Progress in Oceanography*, 136, 50–59, doi:[10.1016/j.pocean.2015.01.001](https://doi.org/10.1016/j.pocean.2015.01.001), 2015.
- 624 Wassmann, P. and Reigstad, M.: Future Arctic Ocean Seasonal Ice Zones and Implications for
625 Pelagic-Benthic Coupling, *Oceanography*, 24(3), 220–231, doi:[10.5670/oceanog.2011.74](https://doi.org/10.5670/oceanog.2011.74), 2011.
- 626 Wu, T., Song, L., Li, W., Wang, Z., Zhang, H., Xin, X., Zhang, Y., Zhang, L., Li, J., Wu, F., Liu,
627 Y., Zhang, F., Shi, X., Chu, M., Zhang, J., Fang, Y., Wang, F., Lu, Y., Liu, X., Wei, M., Liu, Q.,
628 Zhou, W., Dong, M., Zhao, Q., Ji, J., Li, L. and Zhou, M.: An overview of BCC climate system
629 model development and application for climate change studies, *Acta Meteorol Sin*, 28(1), 34–56,
630 doi:[10.1007/s13351-014-3041-7](https://doi.org/10.1007/s13351-014-3041-7), 2014.
- 631 Yu, L., X. Jin, and R. A. Weller, Multidecade Global Flux Datasets from the Objectively Analyzed
632 Air-sea Fluxes (OAFlux) Project: Latent and sensible heat fluxes, ocean evaporation, and related
633 surface meteorological variables. Tech. Report Woods Hole Oceanographic Institution, OAFlux
634 Project Technical Report. OA-2008-01, 64pp. Woods Hole. Massachusetts (2008).



Tables and Figures

Table 1. Linear trends in ice retreat and freeze-up dates (2000–2200), and long-term freeze-up amplification ratios for the individual and mean CMIP5 models and for the 1D model. Trends and ratios are given as median \pm interquartile range over the seasonal ice zone where trends are significant at a 95% confidence level ($p = 0.05$).

	r_r (days / decade)	r_f (days / decade)	$R_{f/r}^{long}$	<i>Reference</i>
CCSM4	-6.6 ± 2.1	13.4 ± 7.3	2.0 ± 0.6	<i>Gent et al., 2011</i>
CNRM-CM5	-8.0 ± 2.8	13.5 ± 5.9	1.7 ± 0.3	<i>Voltaire et al., 2013</i>
CSIRO-Mk3-6-0	-6.1 ± 3.3	10.4 ± 4.0	1.7 ± 0.6	<i>Rotstayn et al., 2012</i>
GISS-E2-H	-2.8 ± 0.6	5.1 ± 1.6	1.8 ± 0.4	<i>Schmidt et al., 2014</i>
MPI-ESM-LR	-8.6 ± 2.8	15.2 ± 8.1	1.8 ± 0.4	<i>Giorgetta et al., 2013</i>
bcc-csm1-1	-5.2 ± 1.3	9.7 ± 2.6	1.9 ± 0.4	<i>Wu et al., 2014</i>
GISS-E2-R	-2.0 ± 0.4	3.4 ± 0.8	1.8 ± 0.3	<i>Schmidt et al., 2014</i>
HadGEM2-ES	-9.1 ± 3.0	18.6 ± 7.6	1.9 ± 0.5	<i>Collins et al., 2011</i>
IPSL-CM5A-LR	-5.7 ± 1.2	11.1 ± 3.8	1.9 ± 0.5	<i>Dufresne et al., 2013</i>
MEAN CMIP5	-6.0 ± 2.0	11.1 ± 4.6	1.8 ± 0.4	
1D model	$-3.1 \pm \text{n.a.}$	$6.0 \pm \text{n.a.}$	$1.9 \pm \text{n.a.}$	



Figure 1. Evolution of the ice seasonality diagnostics (ice retreat date, blue; and freeze-up date, orange):(a) CMIP5 median and interquartile range, with corresponding range of satellite derived-values (green rectangles 1980-2015) over the 70-80°N latitude band; (b) one-dimensional ice-ocean model results. The ice-free period (L_w), the photoperiod (L_p) and the average polar night (gray rectangle) are also depicted. Note that the systematic difference between observations and CMIP5 models is reduced when accounting for the systematic bias due to the daily interpolation of monthly means in CMIP5 models (See Methods and Tab. S2).

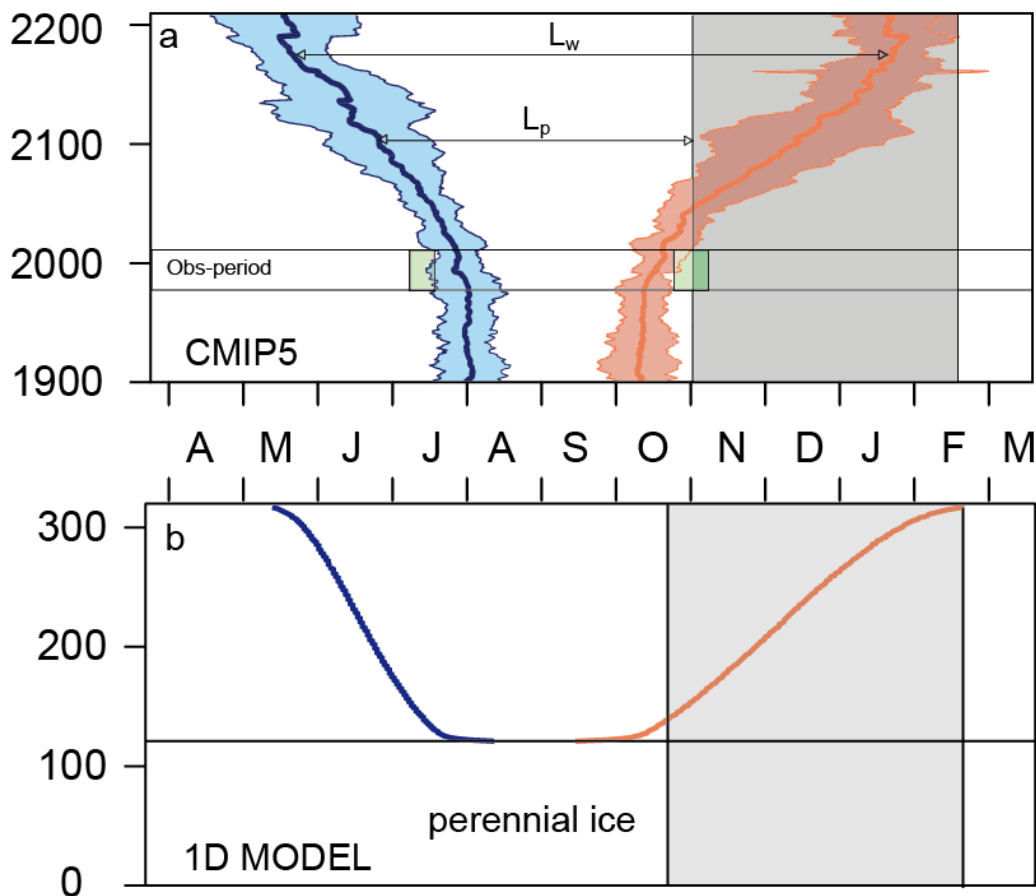




Figure 2. Maps and frequency histograms of (a,d) ice retreat date (b,e) freeze-up date and (c,f) ice-free season length over 1980-2015 (36 years), based on (a,b,c) passive microwave satellite concentration retrievals (Comiso, 2000; updated 2015) and (d,e,f) daily concentration fields averaged over CMIP5 models. Median \pm IQR refers to all points in the seasonal ice zone.

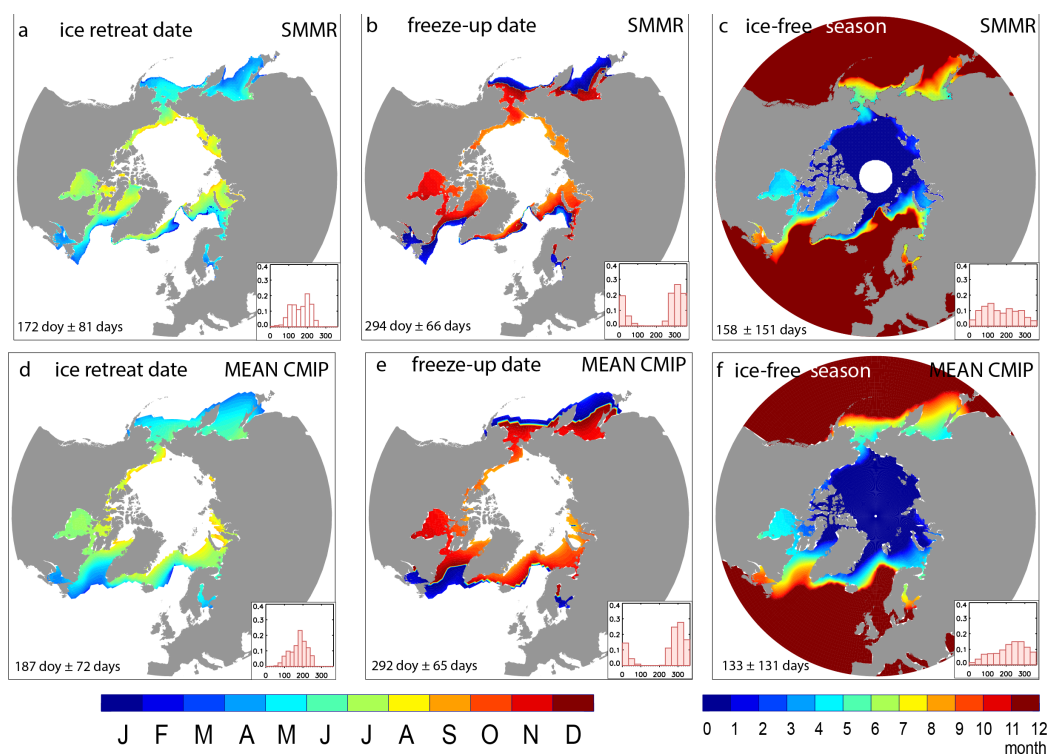




Figure 3. Maps and frequency histograms of linear trends (for Hatched zones only) in (a,d) ice retreat date (b,e) freeze-up date and (c,f) ice-free season length-over 1980-2015 (36 years), based on (a,b,c) passive microwave satellite concentration retrievals (Comiso, 2000; updated 2015); (d,e,f) the mean CMIP5 models. Hatching refers to the 95% confidence interval ($p=0.05$). Median \pm IQR refers to significant pixels with at least 1/3 of the years with defined retreat and freeze-up dates.

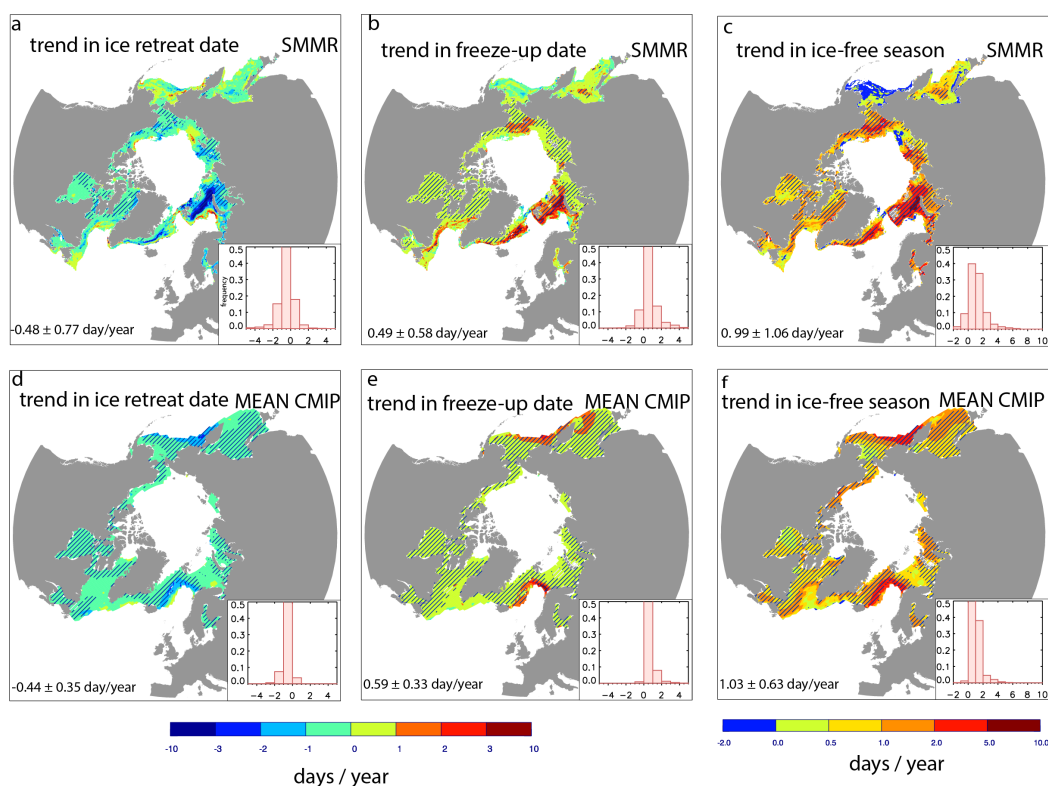




Figure 4. Long-term freeze-up amplification ratio ($p=0.25$) for (a) passive microwave retrievals over 1980-2015; and for IPSL-CM5A-LR simulation over (b) 1980-2015, (c) 2015-2050, (d) 2050-2085. We use a 75% ($p=0.25$) confidence interval for this specific computation.

The same figures for (i) all individual models and (ii) $p = 0.05$ are available as Supplementary Material (Fig. S3 and S7).

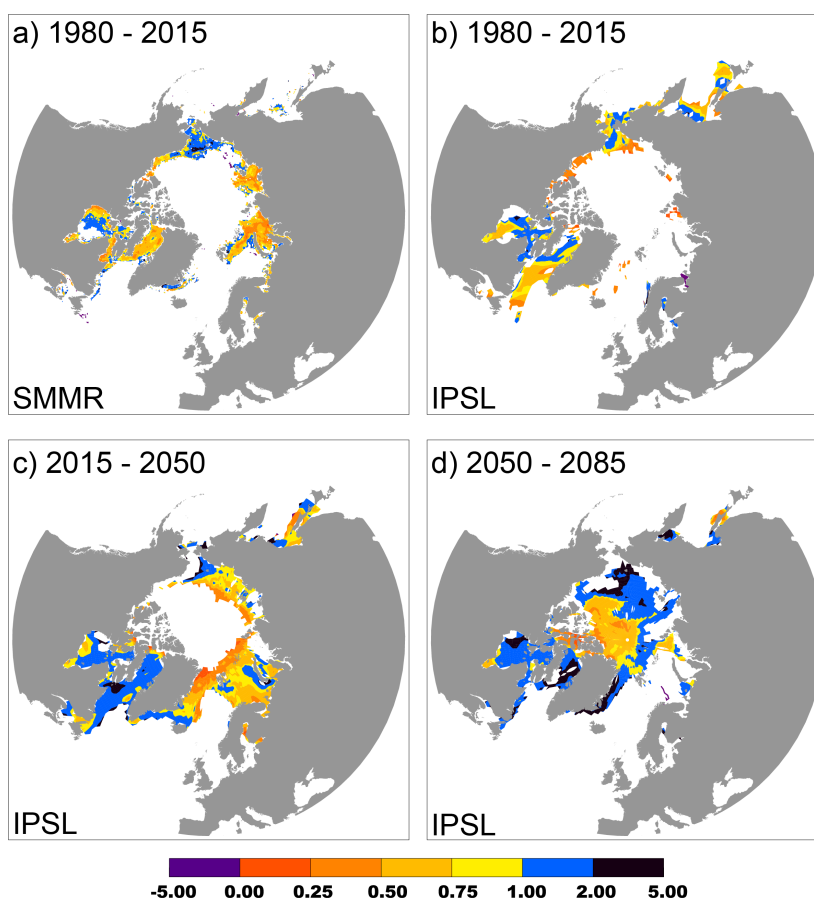




Figure 5. Short-term freeze-up amplification ratio from (a) passive microwave ice concentration retrievals (1980-2015); and from IPSL-CM5A-LR simulated ice concentration fields over (b) 1980-2015, (c) 2015-2050, (d) 2050-2085. Similar maps for all individual models are available as Supplementary Material (Fig. S4).

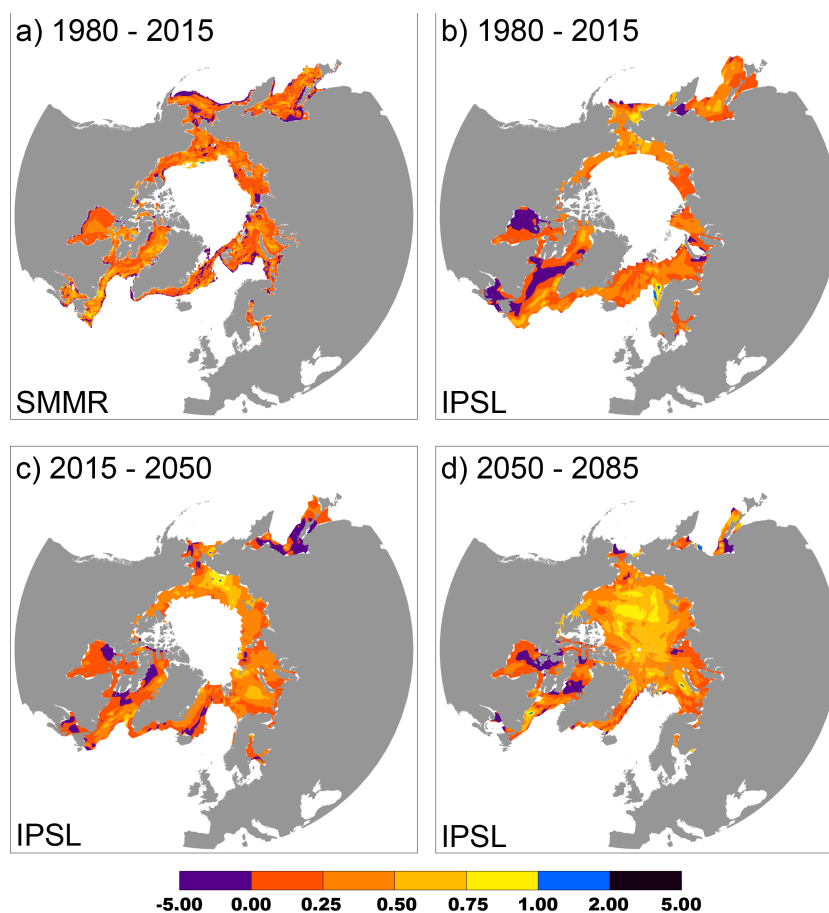




Figure 6. (Top) Energetics of ice retreat and freeze-up in the simple model: net atmospheric (solid) and solar (yellow) heat fluxes to the ocean; SST (dash), depicted for years 150 and 210. **(Bottom)** Annual evolution of the simulated sea surface temperature, averaged over the seasonal ice zone, for two decades of reference (2015-2025, 2075-2085) as simulated by the IPSL_CM5A_LR model and showing the same temporal asymmetry as in the simple model.

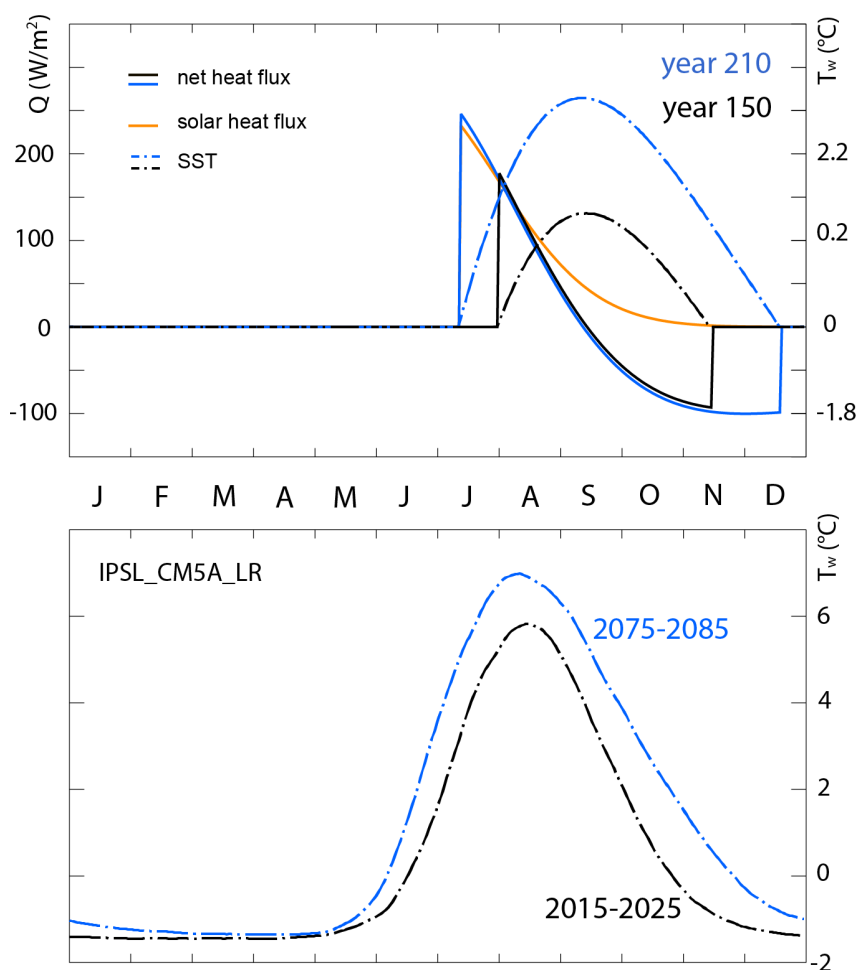




Figure A1. Correspondence between the long-term freeze-up amplification ratio $R_{f/r}^{long}$ and the ice-free ocean energy budget, based on the 1D model. Red circles: direct diagnostic $\Delta d_f / \Delta d_r$ derived from annual time series of d_r and d_f . Orange line: water energetics-derived diagnostic, exact solution, i.e. (10) divided by Δd_r . Blue line: simplified water energetics-derived diagnostic, i.e. (11) divided by Δd_r .

